

A Particle Simulation of 2-D Vessel Motions Interacting with Liquid-Sloshing Cargo

Byung-Hyuk Lee¹, Se-min Jeong², Sung-Chul Hwang², Jong-Chun Park³,
Moo-Hyun Kim⁴

Abstract: The violent free-surface motions interacting with floating vessels containing inner liquid tanks are investigated by using the newly developed Moving Particle Semi-implicit (MPS) method for 2-dimensional incompressible flow simulation. In the present numerical examples, many efficient and robust algorithms have been developed and applied to improve the overall quality and efficiency in solving various highly nonlinear free-surface problems and evaluating impact pressures compared to the original MPS method proposed by Koshizuka and Oka (1996). For illustration, the improved MPS method is applied to the simulation of nonlinear floating-body motions, violent sloshing motions and corresponding impact loads, and vessel motions with inner liquid tanks. It is seen that the roll amplitudes can be significantly reduced due to the presence of the sloshing tank when the excitation frequencies are away from the lowest sloshing natural frequencies. The developed numerical tools can be used to the study of vessel motions with liquid cargo or design of passive anti-rolling devices.

Keywords: Moving Particle Simulation (MPS) method, Free-roll decay, Impact loads, Vessel-motion/Liquid-sloshing interaction, Reduction of roll angle.

1 Introduction

In design of ships and offshore structures, it is of significant importance to accurately predict highly nonlinear free-surface flow motion and the corresponding impact loads, such as large amplitude of waves, liquid sloshing, bow/deck slamming, or green-water problems. It has been recognized that the numerical handling of

¹ Hyundai Maritime Research Institute, Hyundai Heavy Industry, Ulsan, Korea.

² Dept. of Naval Architecture & Ocean Engineering, Pusan National University, Busan, Korea.

³ Dept. of Naval Architecture & Ocean Engineering, Pusan National University, 63-2 Busandaehak-ro, Geumjeong-gu, Busan, Korea.

Tel.: +82-51-510-2480. Fax.: +82-51-583-2485. E-mail: jcpark@pnu.edu.

⁴ Dept. of Civil Engineering, Texas A&M University, Texas, U.S.A.

highly nonlinear free-surface motion interacting with floating body is usually very difficult and challenging because of the complexity associated with fully-nonlinear free-surface and body boundary conditions. There are several CFD (Computational Fluid Dynamics) techniques to handle such problems, i.e. SOLA-VOF (Hirt et al., 1981), Level-Set (Sussman et al., 1994), Marker-Density function (Miyata et al., 1995) etc. Most of them are the techniques capturing the free surface on grid system. However, there is a different approach without grid system, so-called particle method by use of kernel function and Lagrangian treatment of particles. For example, Koshizuka et al. (1996, 1998), Sueyoshi and Naito (2003) developed MPS (Moving Particle Semi-implicit) method, while Monaghan (1988) and Dalrymple and Rogers (2006) used SPH (Smoothed Particle Hydrodynamics). Also, Idelsohn, Onate and Del Pin (2004) developed PFEM (Particle Finite Element Method) for incompressible flows with breaking waves. In MPS method, kernel-function-based difference algorithms are used for differentiation but kernel functions are directly differentiated in SPH method. Also for the pressure calculation the Poisson equation is used and solved iteratively at each time step in MPS method, while the state equation is used in SPH method. It is well known that there are pros and cons in both MPS and SPH methods compared to each other.

The MPS method was originally proposed by Koshizuka and Oka [4] for incompressible flow. In the original MPS method, however, there were several defects including non-optimal source term, gradient and collision models, and search of free-surface particles, which led to less-accurate fluid motions and non-physical pressure fluctuations pointed out by Khayyer and Gotoh (2009, 2011) and Lee et al. (2011).

In the present study, we used a refined MPS (Pusan-National-University-modified MPS, PNU-MPS) method by Lee et al. (2011), in which all the above defects are improved, to study the vessel motions with inner liquid tank and to see the effects of liquid sloshing on vessel motions. The coupling between ship motion and sloshing has been studied by Molin et al. (2002), Kim (2002), Malenica et al. (2003), Rognbakke and Faltinsen (2003), and Newman (2005) based on linear potential theory in the frequency domain. In time domain, Kim et al. (2003, 2007) studied the sloshing effect on the motion of a single ship with 2-D and 3-D viscous FDM (Finite Difference Method) sloshing codes. Lee et al. (2007, 2008) and Kim et al. (2011) also investigated the sloshing effect of multiple tanks on ship's roll motions with 3-D FDM and MPS sloshing calculations, respectively. In this study, it is shown that the PNU-MPS method can be applied to the prediction of vessel motion with liquid cargo and the design of passive liquid-tank-based anti-rolling devices.

2 Moving Particle Simulation

2.1 Governing Equation

The Governing equations for incompressible viscous flows are the continuity and Navier-Stokes equations as follows:

$$\frac{D\rho}{Dt} = 0 \quad (1)$$

$$\frac{D\vec{u}}{Dt} = -\frac{1}{\rho}\nabla P + \nu\nabla^2\vec{u} + \vec{F} \quad (2)$$

The symbol ρ is the density, t the time, \vec{u} the velocity vector, ∇ the gradient, P the pressure, ν the kinematic viscosity, and \vec{F} the external force.

The left-hand side of Navier-Stokes equation (2) denotes Lagrangian differentiation that is directly calculated by moving particles in a Lagrangian manner. The right-hand sides consist of pressure gradient, viscous, and external-force terms. To simulate incompressible flows, all terms expressed by differential operators should be replaced by the particle interaction models of the MPS method. In the present paper, the refined MPS (PNU-MPS) method is used for all simulation, which can calculate the flow field with violent free-surface motion more accurately and stably compare to the original MPS proposed by Koshizuka and Oka (1996).

2.2 Kernel Function

Continuous fluid can be represented by physical quantities of coordinates, mass, velocity components, and pressure for particles. The governing equations written with partial differential operators are transformed to the equation of particle interactions. The particle interactions in the MPS method are based on a kernel function. In this study, the following functions are employed:

$$w(r) = \begin{cases} \left(1 - \frac{r}{r_e}\right)^3 \left(1 + \frac{r}{r_e}\right)^3 & (0 \leq r < r_e) \\ 0 & (r_e < r) \end{cases} \quad (3)$$

The distance between two particles is r and r_e represents the effective range of particle interactions. The kernel becomes zero where $r > r_e$. Since the area covered with this weight function is bounded, a particle interacts with a finite number of neighboring particles. The radius of the interaction area is determined by the parameter, r_e . The weighting of interaction between two particles can be described by the kernel function; i.e. the nearer the distances between two particles, the larger the weight of interactions. If the distance between two particles is quite long, their interactions can be neglected. The kernel (3) seems to be more robust and gives

more reasonable interaction between neighboring particles for the weakly-violent free-surface problem than that used in the original MPS method (Koshizuka and Oka, 1996).

2.3 Gradient Model

A gradient vector between two particles i and j possessing scalar quantities φ_i and φ_j at coordinates r_i and r_j is defined as $(\varphi_j + \varphi_i) (\vec{r}_j - \vec{r}_i) / |\vec{r}_j - \vec{r}_i|^2$ based on the action-reaction physical law (Toyota et al., 2005). The gradient vector at the particle i is given by the weighted average of these gradient vectors:

$$\langle \nabla \varphi \rangle_i = \frac{d}{n^0} \sum_{i \neq j} \left[\frac{\varphi_j + \varphi_i}{|\vec{r}_j - \vec{r}_i|^2} (\vec{r}_j - \vec{r}_i) w(|\vec{r}_j - \vec{r}_i|) \right] \quad (4)$$

where d is the number of space dimensions and n^0 is the particle number density fixed for incompressibility of the initial condition of particle arrangement. The particle number density is calculated by the following equation.

$$n_i = \sum_{i \neq j} w(|\vec{r}_j - \vec{r}_i|) \quad (5)$$

The fluid density is proportional to the particle number density.

2.4 Laplacian Model

The diffusion of φ at particle i is described by

$$\nabla^2 \varphi = \frac{2d}{\lambda} (\varphi_j - \varphi_i) w(|r_j - r_i|) \quad (6)$$

$$\lambda = \frac{\sum_{j \neq i} w(|\vec{r}_j - \vec{r}_i|) |r_j - r_i|^2}{\sum_{j \neq i} w(|\vec{r}_j - \vec{r}_i|)} \cong \frac{\int_V w(r) r^2 dv}{\int_V w(r) dv} \quad (7)$$

where λ is the parameter by which the variance increase is equal to that of the analytical solution.

2.5 Incompressibility Model

Fluid density is represented by the particle number density. Thus, the continuity equation (1) is fulfilled with fixing the particle number density through the simulation. This means that the particle number density n^0 should be constant.

The algorithm of incompressibility for the MPS method is similar to that of the SMAC (Simplified Marker-and-Cell) method in grid system. In each time step, there are two stages: in the first stage, the temporal velocity components \vec{u}_i^* is obtained using diffusion, external forces, and convection terms, which are explicitly calculated with the values in the (n)-th time step.

In the second stage, the Poisson equation for pressure is calculated implicitly (Tanaka and Masunaga, 2008):

$$\nabla^2 P_i = (1 - \gamma) \frac{\rho}{\Delta t} \nabla \cdot \vec{u}_i^* + \gamma \frac{\rho}{\Delta t^2} \frac{n^0 - n_i^n}{n^0} \quad (8)$$

The blending coefficient γ of the right-hand side of (8) is less than 1.0 and the range of $0.01 < \gamma < 0.05$ is recommended in Lee et al. (2011).

The left-hand side of (8) is discretized by the Laplacian model (6). The first source term of Eq. (8) is the divergence-free condition and calculated by the following equation:

$$\langle \nabla \cdot \vec{u} \rangle_i = \frac{d}{n^0} \sum_{i \neq j} \left[\frac{(\vec{u}_j - \vec{u}_i) \cdot (\vec{r}_j^\rightarrow - \vec{r}_i^\rightarrow)}{|\vec{r}_j^\rightarrow - \vec{r}_i^\rightarrow|^2} w(|\vec{r}_j^\rightarrow - \vec{r}_i^\rightarrow|) \right] \quad (9)$$

And the second source term of Eq. (8) is represented by the deviation of the particle number density from the constant and means that the particle number densities should be maintained during the simulation.

In Eq. (8), we have simultaneous equations expressed by a linear symmetric matrix and they are solved by iteration method. In the present study, the CG (Conjugate Gradient) method is employed as the iterative solver.

After updating the pressure field, the velocity correction \vec{u}'_i is calculated by the following equation:

$$\vec{u}'_i = -\frac{\Delta t}{\rho} \langle \nabla P^{n+1} \rangle \quad (10)$$

Finally, the velocity components and coordinates of particles in the (n + 1)-th time step are calculated from the following equations:

$$\vec{u}_i^{n+1} = \vec{u}_i^n + \vec{u}'_i \quad (11)$$

$$\vec{r}_i^{n+1} = \vec{r}_i^n + \Delta t \vec{u}_i^{n+1} \quad (12)$$

2.6 Boundary Condition

As the free-surface boundary condition, the kinematic and dynamic boundary conditions are imposed on the free-surface particles. The kinematic condition can be directly satisfied by moving particles on the free-surface. In the present method, it is straightforward to track the free-surface particles because the location of the free-surface is easily obtained as a result of the fully Lagrangian treatment of particles.

In the vicinity of the free-surface, the particle number densities are decreased because of including the empty air region, where no particles exist in case of single-phase problem. Thus, on the free surface, the particles satisfying the following simple conditions are considered:

$$\langle n \rangle_i^* < \beta_1 n^0 \quad (13)$$

$$N_i < \beta_2 N^0 \quad (14)$$

In the above equations, β_1 and β_2 are parameters below 1.0, N_i the number of neighboring particles within effective range of particle interaction r_e and N_0 the maximum number of neighboring particles for fully submerged particles in the initial distribution. Especially, the free-surface parameter β s are used to judge whether the particles are on the free-surface or not, and β_1 and β_2 are set at 0.97 and 0.85 respectively in this study, which are used in Lee et al. (2011). Using this free-surface boundary condition, the simulation of fragmentation and coalescence of free-surface flow is available.

Assuming that there is no viscosity at the free-surface, the dynamic free-surface condition is satisfied by taking the atmospheric pressure ($P = P_{atm} = 0$) on the free-surface particles. This condition is fulfilled in the procedure of solving the Poisson equation (8).

The wall particles are set along the solid boundary and dummy particles are placed inside the solid wall. In particle method, it is important to get the useful information of physical quantities from the neighboring particles. The physical quantities are calculated through interaction with those of neighboring particles. The wall particles are directly in contact with both the fluid and dummy particles. They are involved in the pressure calculation and prevent the concentration of particles near the wall. Also, they have zero velocities treated as no-slip on wall. Three layers of particles are located to ensure that the particle number density is computed accurately.

2.7 Collision Model

When particles get close inside fluid, repulsive force due to the local pressure can be calculated without introducing any special collision model. For the particles on the free surface, however, the pressure is fixed by the constant atmospheric pressure, and thus, repulsive forces are not properly generated even when particles get close. In particular, when the particles accelerated from outside collide with free surface, the number density can suddenly be increased. As a result, it may not be recognized as a free-surface particle, so the pressure can be suddenly increased. This phenomenon greatly reduces the spatial stability of the pressure. Therefore, a special collision model needs to be employed to better represent the proper repulsive forces especially near the free surface.

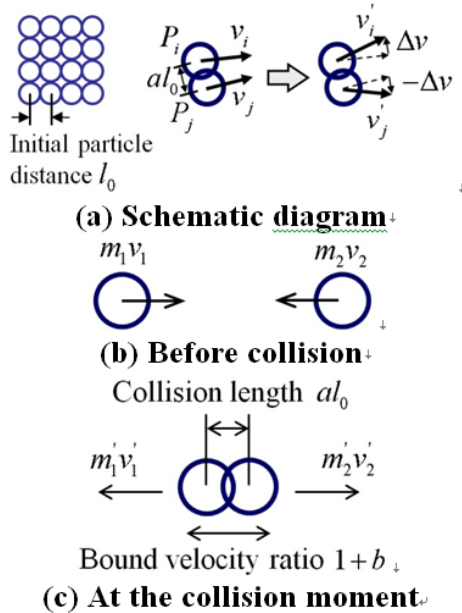


Figure 1: Diagram of collision model.

Figure 1 shows a simple diagram for the collision model. In the beginning, the particles are uniformly distributed with constant distance of l_0 . When the distance between any two particles gets smaller than al_0 , the collision model is applied. Then, from the conservation of momentum, the repulsive velocity can be calculated by using the coefficient $1 + b$, which is defined as the ratio of $b = -\vec{v}' / \vec{v}$. The range of good performance of $a > 0.85$ and $b < 0.2$ was recommended in Lee et al. (2011).

2.8 Numerical Treatment of Motion of Floating Body

In this section, a numerical treatment for solving the motion of floating body is introduced. Koshizuka and Oka (1996) proposed a passively moving-solid model to describe the motion of a rigid body in a fluid. Here, a solid is assumed as a collection of particles held together by intermolecular forces. At first, the solid particles are calculated with the same incompressible algorithm of fluid particles. In this stage the coupling effect between the individual solid particles is not considered. As a result of the simulation for this stage the solid deforms, so relative locations of the solid particles should be corrected by the equations below.

At the center of rigid body, the translational velocity, \vec{T} , and rotational velocity, \vec{R} , are calculated as given in the following equations:

$$\vec{T} = \frac{1}{n} \sum_{i=1}^n \vec{u}_i \quad (15)$$

$$\vec{R} = \frac{1}{I} \sum_{i=1}^n \vec{u}_i \times \vec{q}_i \quad (16)$$

Here, the relative coordinates between solid particles, \vec{q}_i , and the moment of inertia, I , are given as:

$$\vec{q}_i = \vec{r}_i - \vec{r}_g \quad (17)$$

$$I = \sum_{i=1}^n |\vec{q}_i|^2 \quad (18)$$

Here, \vec{r}_g is the center of gravity and calculated as follows:

$$\vec{r}_g = \frac{1}{n} \sum_{i=1}^n \vec{r}_i \quad (19)$$

Finally, the velocity vector of the solid particles are replaced by

$$\vec{u}_i = \vec{T} + \vec{q}_i \times \vec{R} \quad (20)$$

In the next time step, the fluid particles are slightly affected by this solid motion through the incompressibility calculation.

3 Numerical results and discussions

3.1 Floating -body Simulation

To verify the simulation of a floating body with free-surface, the motions of a 2D floating rectangular barge in a numerical water-filled (density=1000kg/m³) wave

tank were simulated in time domain by using the passively moving-solid model. The dynamic characteristics, i.e. damping coefficient and natural frequency, were calculated from the numerical simulation and these values were compared with those by experiment (Jung et al., 2006).

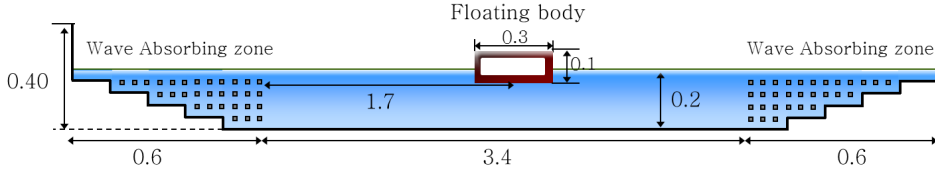


Figure 2: Initial configuration for simulating motions of 2D rectangular barge.

The initial geometry and set-up are shown in Figure 2. The width and height of the numerical wave tank are 4.6m and 0.4m, respectively. The top of the tank is opened and the water depth is 0.2m. To reduce the reflecting waves, 0.6m length wave absorbing zones were placed near the side boundaries. The width and height of the floating body are 0.1m and 0.3m. The draft and metacentric height (GM) of the body were 0.05m and 0.125m, respectively. The initial distance between particles, l_0 , is 0.01m and the total number of particles used for the simulation is 8,406. Initially, the body is forced to be rotated counter-clockwise 15 degrees. In this study, only the roll motion (1 degree of freedom) of the body, which can be expressed as (21) in the calm water condition, is considered.

$$\frac{d^2\varphi}{dt^2} + 2\zeta\omega_N\frac{d\varphi}{dt} + \omega_N^2\varphi = 0 \quad (21)$$

Here, φ , ζ and ω_N are the roll(inclined) angle, damping coefficient and natural frequency of the body, respectively.

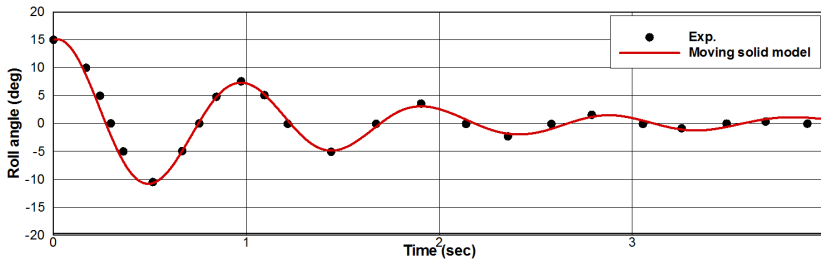


Figure 3: Time history of roll angles.

Figure 3 shows the corresponding time histories of the roll motions obtained by experiment and present numerical simulation using the passively moving-solid model. The roll angles decay exponentially for both experiment and numerical simulation. Although small discrepancies in the roll angle and periods exist, it can be said the simulation result using the moving-solid model agrees well with that by experiment.

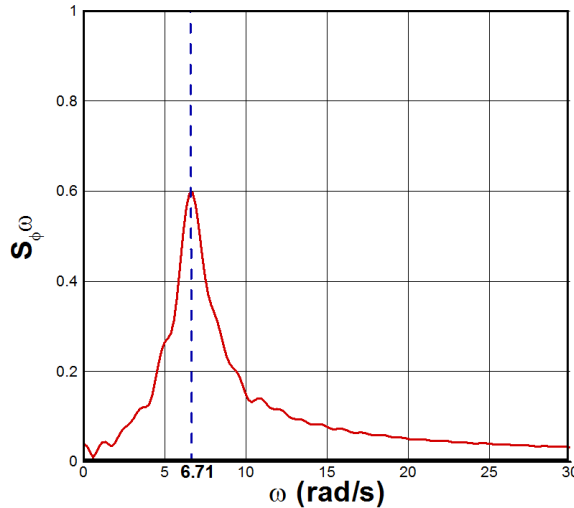


Figure 4: Energy spectra with the roll natural frequency with adopting the simulations result.

Table 1: Comparison of natural frequencies(ω_N) and damping coefficients(ζ)

	ω_N (rad/s)	Error (%)	ζ (rad/s)	Error (%)
Experiment	6.78	-	0.106	-
Simulation	6.71	1.03	0.011	7.03

As for the quantitative comparison, firstly, the natural frequency for the simulation was computed through the spectrum of the recorded time history as depicted in Figure 4. And then, following to Bhattacharyya (1978), the damping coefficient was estimated from the slope of the extinction curve, which shows the decrease of inclination for each single roll plotted against the interpolated inclination (called the mean angle of roll, φ_m) for the body, as shown in Figure 5. The computed values are summarized in the Table 1. The natural frequency of roll motion is

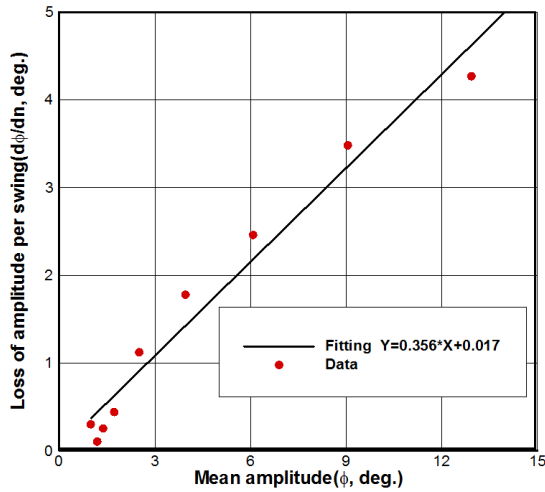


Figure 5: Curves of extinction with adopting the simulation result.

well predicted with approximately 1% error by the numerical simulation compared to that of experiment. The error of damping coefficients between the experiment and the simulation with adopting the moving-solid model is about 7%, which is thought to be acceptable for engineering purposes. The moving-solid model is simple and computationally economical, and for the ensuing examples of this paper, the passively moving-solid model will be employed to calculate the motion of a floating body.

3.2 Validation for prediction of impact pressure by sloshing

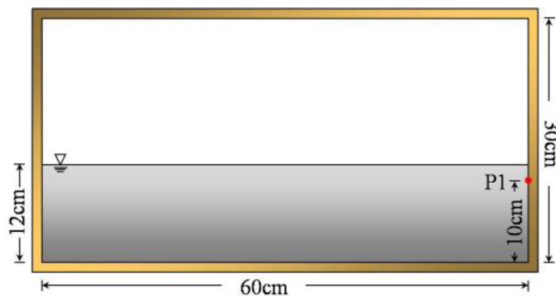


Figure 6: Schematic view of tank dimension and position of pressure gauge.

We consider the water sloshing problem inside a 2D rectangular tank driven by a harmonic oscillator. The simulation results are compared with the experimental results of Kishev et al. (2006). The experimental set-up is shown in Figure 6. The tank width and height are 0.6m and 0.3m, respectively. The water depth is 0.12m. The tank is forced to move sinusoidally in the horizontal direction as follows:

$$X_H = A \sin(2\pi/Tt) \quad (22)$$

where the oscillation amplitude $A=0.05\text{m}$ and the period $T=1.3\text{s}$.

The total number of particles used for the present simulation is 4000, among which fluid particles are 3000. The gravitational acceleration and water density are set at 9.81m/s^2 and 1000kg/m^3 and the surface tension is neglected. The kinematic viscosity of water (ν) is given by $\cong 10^{-6}\text{m}^2/\text{s}$ and the total computational time is 16s. The collision-model coefficients a and b used for this simulation are 0.9 and 0.2. To compare with the pressure measurement of Kishev et al. (2006), the reference point P1 on the right-side wall is selected, as shown in Figure 6.

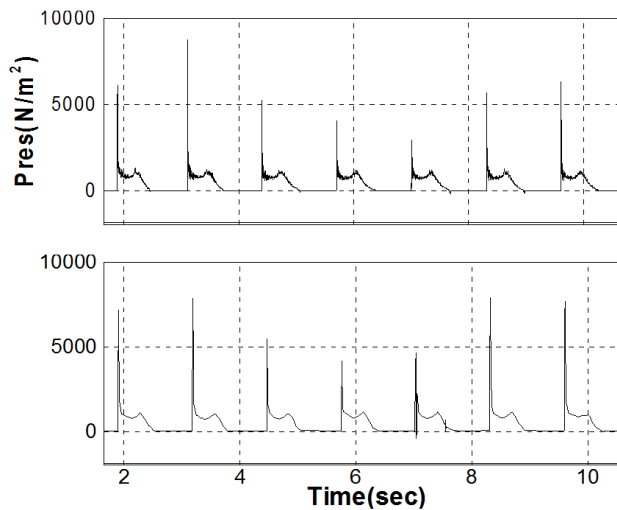


Figure 7: Comparison of sloshing-induced impact pressure profiles (top=PNU-MPS and bottom=experiment of Kishev et al. (2006): $\cong 1.3\text{sec}$).

Figure 7 shows the comparison between experimental and simulated impact-pressure time histories at P1 for $T=1.3\text{s}$. The primary peaks are caused by the initial water slamming onto the vertical wall, while the small secondary peaks are due to the fall of water splash along the wall. The trend of the pressure signal between experiment

and simulation is very similar. The mass is conserved for a very long time by the present PNU-MPS method, and thus long-time simulation is possible to investigate the statistical properties of the peaks. It also needs to be pointed out that the sloshing experiment itself is not completely repeatable/reproducible showing different peak values at each trial. There also exists 3D effect in the experiment, so perfect match up to measurement is impossible.

3.3 Vessel/Liquid-Sloshing Interaction and Impact Loads

In the previous two sections, we validated independently the simulations of floating bodies with free surface, and the violent sloshing motions of water inside a tank and the corresponding impact loads. Now, let us investigate how the motion of a floating body is changed when it has a partially-filled inner liquid tank like LNG carriers. The inner liquid tank can also be used as a passive anti-rolling tank. In this regard, the vessel/liquid-sloshing interactions and the corresponding impact loads acting on the wall are investigated by using the PNU-MPS. The initial geometry and set-up are shown in Figure 8. The floating body is initially positioned at the center of the outer tank which is forced to move sinusoidally in the horizontal direction by (22) to provide harmonic excitations. In a very simple approach, one can only add the mass of water cargo to the mass of floating body and solve the equation of motion like a solid cargo with the correction of hydrostatic restoring coefficients due to the inner free surface. In the simple approach, the hydrodynamic effects of the inner-water sloshing motion, for example that associated with the added mass of the inner water, are neglected. In this regard, we compared two different cases; when the liquid cargo is treated as (i) solid cargo and (ii) liquid with sloshing motions. The breadth, height, and thickness of the sloshing tank are 0.40m, 0.20m, and 0.03m, respectively. The filling ratio and cargo material inside the sloshing tank are varied as in Table 2. The breadth and water depth of the outer tank are 1.50m and 0.25m, respectively. Its oscillation amplitude $A=0.02\text{m}$ and period $T=0.9\text{s}$, 1.2s , and 2.0s . The two periods, 0.9s and 1.2s , are close to the analytical (linear potential theory) natural periods of the lowest sloshing modes at the respective fill-ratios. The density of the water and the floating body are fixed at $1000(\text{kg}/\text{m}^3)$. The total number of particles used for this simulation is 5,000. The total calculation time is 30 periods and the surface tension is neglected here for convenience.

Figures 9-16 show the comparisons of the trajectories of roll angles and center positions for Case 1-8. First, Cases 1-4 correspond to the case of external excitation ($T=2\text{s}$) whose frequency is away from the sloshing natural frequencies.

In these cases, we can see that there is significant reduction of roll angles when the solid cargo is replaced by liquid cargo. The reduction rate is larger in Case 2 (50% fill ratio) than in Case 4 (25% fill ratio). Interestingly, there is no apparent

Table 2: Initial condition of the simulation

Cases	Fill ratio (%)	Period (T)	Material
Case 1	50	2.0	Solid
Case 2	50	2.0	Liquid
Case 3	25	2.0	Solid
Case 4	25	2.0	Liquid
Case 5	50	0.9	Solid
Case 6	50	0.9	Liquid
Case 7	25	1.2	Solid
Case 8	25	1.2	Liquid

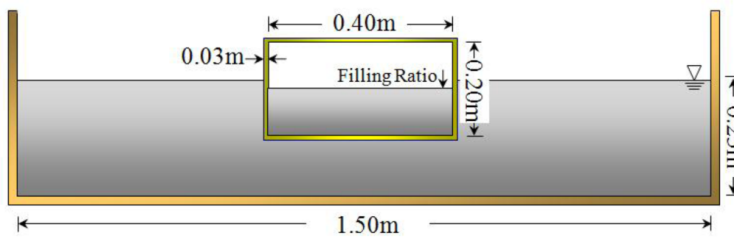


Figure 8: Initial setup for motion of floating body with partially-filled inner liquid tank.

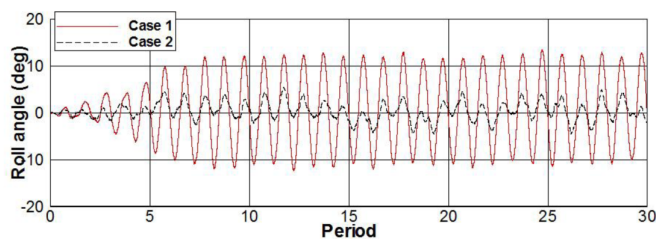


Figure 9: Comparison of roll angle between case 1 and Case 2.

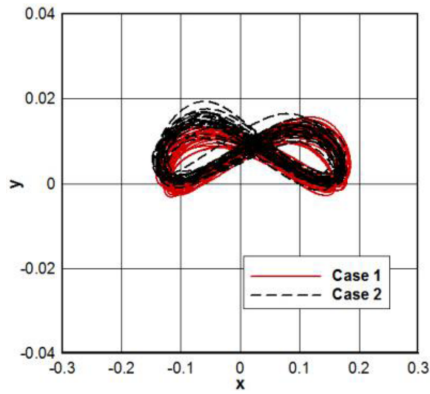


Figure 10: Trajectory of center position for case 1 and case 2.

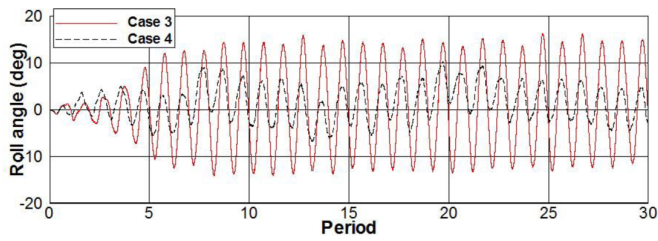


Figure 11: Comparison of roll angle between case 3 and Case 4.

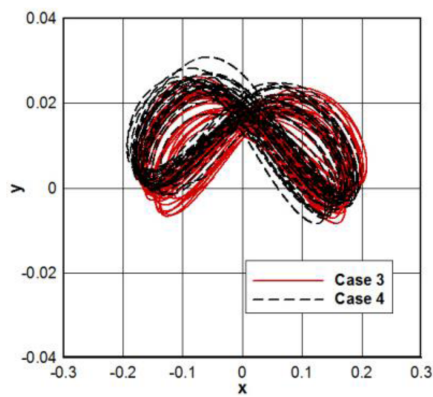


Figure 12: Trajectory of center position for case 3 and case 4.

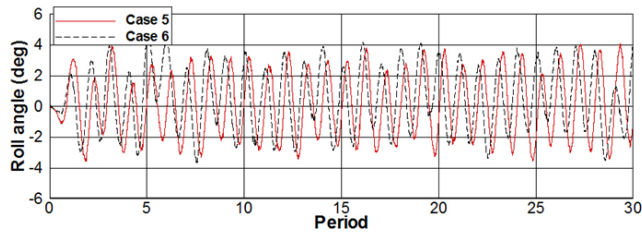


Figure 13: Comparison of roll angle between case 5 and Case 6.

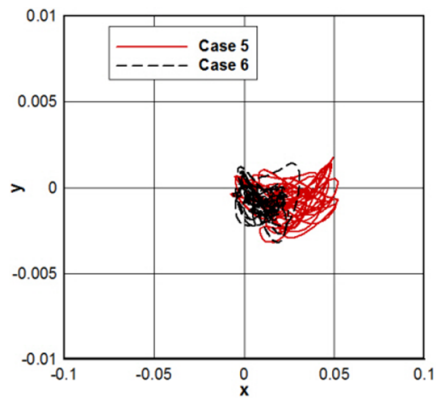


Figure 14: Trajectory of center position for case 5 and case 6.

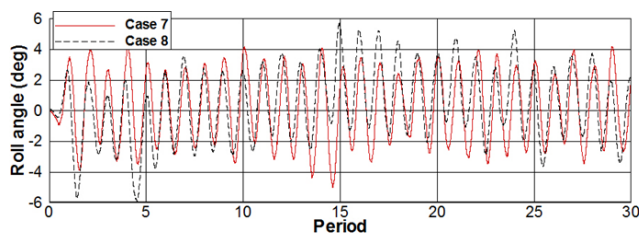


Figure 15: Comparison of roll angle between case 7 and Case 8.

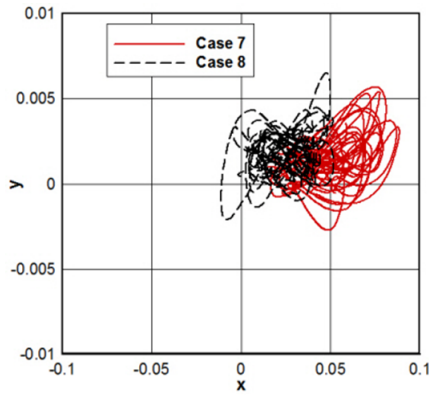


Figure 16: Trajectory of center position for case 7 and case8.

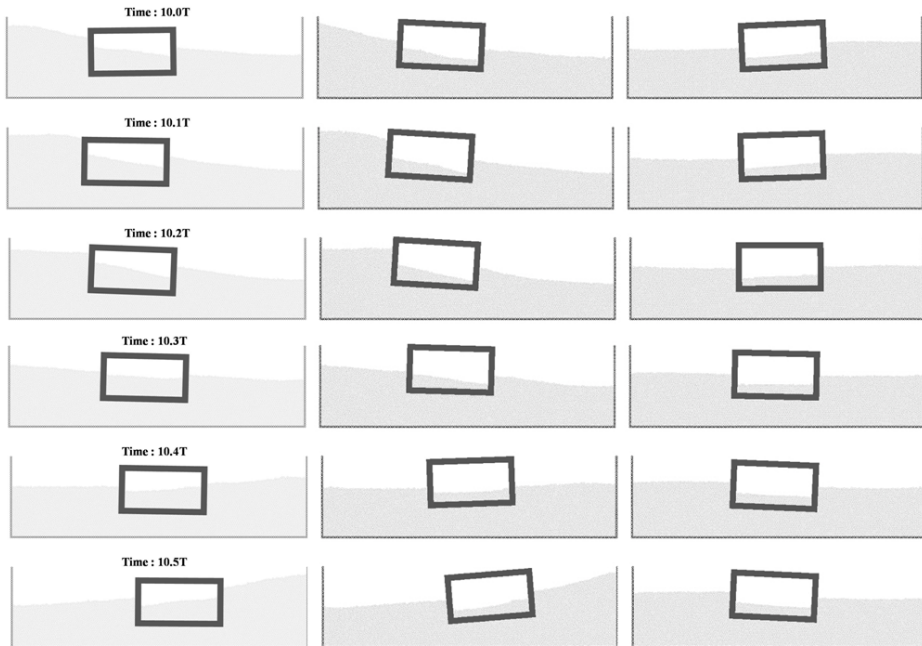


Figure 17: Comparison of Snapshots between Case 2, Case 4 and Case 8.

change in sway and heave motions in both cases. Figures 13-14 correspond to the cases of 5 and 6, for which the excitation frequency ($T=0.9s$) is close to the lowest sloshing frequency of fill ratio=50%. It is seen that the maximum roll angle is

rather increased with liquid tank, while the sway motions and mean sway offset are decreased with including the sloshing effects. Figures 15-16 show the same sets of results for $T=1.2s$, which is close to the lowest natural frequencies of fill ratio=25%. In general, this case shows similar trend compared to Figures 13-14 but the differences between the solid and liquid cargos become more appreciable despite the smaller amount of water inside the tank. It may be due to the fact that the inner sloshing motions of the latter are more violent. Finally, we show, in Figure 17, a series of snap-shots of vessel motions and inner/outer free-surface motions for three different cases. The motions of the outer water of Case 2 and 4 are greater since the oscillation period 2s is close to the lowest sloshing natural frequency of the outer tank. When the vessel motion is significantly reduced, such like Case 2 and 4, the slope of inner free surface follows that of outer free surface.

The CPU time was spent about 50.27s for simulating Case 6 during 30 periods ($T=27s$) using a Intel® Core™ i7-3930K of CPU 3.2GHz and RAM 16Gb.

4 Concluding remarks

A very efficient and robust MPS method has been applied to better predict violent free-surface motions interacting with a floating body containing inner liquid tank as well as the impact pressures on the tank induced by such motions. The floating-body-motion module adopting the passively moving solid-model was verified by conducting a numerical simulation on the roll-motion of a 2-D floating rectangular barge and comparing the simulation results with experimental ones by Jung et al. (2006). The prediction of impact pressures induced by violent sloshing motions in a liquid tank was also independently validated by comparison against experimental results of Kisev et al. (2006). Then a refined MPS program including both floating-body module and liquid-sloshing module was run to observe the effects of the inner-liquid motions on the floating-body motions. It is seen that the roll amplitudes can be significantly reduced due to the presence of the sloshing tank when the excitation frequencies are away from the lowest sloshing natural frequencies. The reduction rate depends on the fill ratio and interestingly, more reduction at 25% fill ratio than that at 50% fill ratio. When the excitation frequencies are close to the lowest sloshing natural frequencies, the maximum roll angles can be slightly increased due to the liquid cargo. The developed numerical tools can be used to the study of vessel motions with liquid cargo or design of passive anti-rolling devices. The developed tool is expected to be very useful for the analysis of the complex and interacting motions between free-surface and floating bodies containing inner liquid tanks, such as LNG (Liquefied Natural Gas) carrier, LNG-FPSO (Floating Production Storage and Offloading), passive anti-rolling device and so forth.

Acknowledgement

This work was supported by the Financial Supporting Project of Long-term Overseas Dispatch of PNU's Tenure-track Faculty, 2009.

References:

- Bhattacharyya, R.** (1978): Dynamic of marine vehicles. John Wiley & Sons Inc, New York.
- Dalrymple, R.A. and Rogers, B.D.** (2006): Numerical Modeling of Water Waves with the SPH Method. *Coastal Engineering*, vol. 53, No. 2-3, pp. 141-147.
- Hirt, C.W.; Nichols, B.D.** (1981): Volume of Fluid (VOF) method for dynamics of free boundaries. *Journal of Computational physics*, vol. 39, pp. 201-225.
- Idelsohn, S.R., Onate, E., Del Pin, F.** (2004): The particle finite element method: a powerful tool to solve incompressible flows with free-surfaces and breaking waves. *Int. J. Numer. Methods Engrg.*, vol. 61, pp. 964-989.
- Jung, K.-H., Chang, K.-A., Jo, H.-J.** (2006): Viscous Effect on the Roll Motion of a Rectangular Structure. *Journal of Engineering Mechanics*, vol. 132, no.2, pp.190-200.
- Khayyer, A., Gotoh, H.** (2009): Modified moving particle semi-implicit methods for the prediction of 2D wave impact pressure. *Coastal Engineering*, vol. 56, pp. 419-440.
- Khayyer, A., Gotoh, H.** (2011): Enhancement of stability and accuracy of the moving particle semi-implicit method. *Journal of Computational Physics*, vol. 230, pp. 3093-3118.
- Kim, K.-S., Lee, B.-H., Kim, M.-H., Park, J.-C.** (2011): Simulation of Sloshing Effect on Vessel Motions by Using MPS (Moving Particle Simulation). *CMES:Computer Modeling Engineering Sciences*, vol. 79, no. 3, pp. 201-221.
- Kim, Y.** (2002): A numerical study on sloshing flows coupled with ship motion-the anti-rolling tank problem. *Journal of Ship Research*, vol. 46, no. 1, pp. 52-62.
- Kim, Y., Shin, Y.S., Lin, W.M., Yue and D.K.P.** (2003): Study on sloshing problem coupled with ship motion in waves. *The 8th International Conference on Numerical Ship Hydrodynamics*, Busan, Korea.
- Kim, Y., Nam, B.W., Kim, D.W., Kim, Y.S.** (2007): Study on Coupling Effect of Ship Motion and Sloshing. *Ocean Engineering*, vol. 34, pp. 2176-2187.
- Kishev, Z., Hu, C. and Kashiwagi, M.** (2006): Numerical simulation of violent sloshing by a CIP-based method. *Journal of Marine Science Technology*, vol. 11, pp. 111-122.

Koshizuka, S., Oka, Y. (1996): Moving-particle semi-implicit method for fragmentation of incompressible fluid. *Numerical Science and Engineering*, vol. 123, pp. 421-434.

Koshizuka, S., Nobe, A. and Oka, Y. (1998): Numerical Analysis of Breaking Waves Using the Moving Particle Semi-implicit Method. *International Journal for Numerical Method in Fluids*, vol. 26, pp. 751-769.

Lee, B.-H., Park, J.-C., Kim, M.-H., Hwang, S.-C. (2011): Step-by-step improvement of MPS method in simulating violent free-surface motions and impact loads. *Comput. Methods Appl. Mech. Engrg.*, vol. 200, pp. 1113-1125.

Lee, B.-H., Park, J.-C., Kim, M.-H., Hwang, S.-C. (2011): Moving Particle Simulation for Mitigation of Sloshing Impact Loads Using Surface Floaters. *Computer Modeling in Engineering and Science*, vol. 75, no. 2, pp. 89-112.

Lee, S.J., Kim, M.H., Lee, D.H., Kim, J.W. and Kim, Y.H. (2007): The effects of LNG-tank sloshing on the global motions of LNG carriers. *Ocean Engineering*, vol. 34, pp. 10-20.

Lee, S.J., Kim, M.H., Shin, Y.S. and Kim, B.K. (2008): The effects of Tank Sloshing on the Coupled Responses of LNG vessel and Floating Terminal. *Proceedings of the Eighteenth (2008) International Offshore and Polar Engineering Conference*, pp. 178-183, Vancouver, Canada.

Malenica, S., Zalar, M., and Chen, X.B. (2003): Dynamic coupling of seakeeping and sloshing. *Proc. 13th Int. Offshore and Polar Eng. Conference*, Hawaii, USA.

Miyata, H., Park, J.C. (1995): Potential Flow of Fluids, ed. M. Rahman, *Computational Mechanics Publications*, UK., pp. 149-176.

Molin, B., Remy, F., Rigaud, S., and de Jouette, Ch. (2002): LNG-FPSO's: frequency domain, coupled analysis of support and liquid cargo motion. *Proceedings IMAM Conf.*, Rethymnon, Greece.

Monaghan, J.J. (1988): An Introduction to SPH. *Comput. Phys. Comm.*, vol. 48, pp. 89-96.

Newman, J.N. (2005): Wave effects on vessels with internal tanks. *The 20th Workshop on Water Waves and Floating Bodies*, Spitsbergen.

Rognebakke, O.F., Faltinsen, O.M. (2003): Coupling of sloshing and ship motions. *Journal of Ship Research*, vol. 47, No. 3, pp. 208-221.

Sueyoshi, M., Naito, S. (2003): Numerical Study of Violent Free Surface Problems with Particle Method for Marine Engineering. *Proc. 8th International Conference on Numerical Ship Hydrodynamics*, Busan, vol. 2, pp 330-339.

Sussman, M., Smereka, P. and Osher, S. (1994): A Level Set Approach for Computing Solutions to Incompressible Two-Phase Flow. *Journal of Computational*

Physics, vol. 114, pp. 272-280.

Toyota, E., Akimoto, H. and Kubo, S. (2005): A particle method with variable spatial resolution for incompressible flows. *19th Japan Society of Fluid Mechanics*, A9-2.

Tanaka, M. and Masunaga, T. (2008): Stabilization smoothing of pressure on MPS method by quasi-compressibility. *Transactions of the Japan Society for Computational Engineering and Science*, vol. 2008, 20080025. (in Japanese).

